J. Fluid Mech. (1987), *vol.* 179, *pp.* 439–468
Printed in Great Britain

The structure of a turbulent shear layer bounding a separation region

By I. P. CASTRO AND A. HAQUE†
Department of Mechanical Engineering, University of Surrey, Guildford, Surrey GU2 5XH, UK

(Received 22 May 1986)

Detailed measurements within the separated shear layer behind a flat plate normal to an airflow are reported. A long, central splitter plate in the wake prevented vortex shedding and led to an extensive region of separated flow with mean reattachment some ten plate heights downstream. The Reynolds number based on plate height was in excess of 2×10^4.

Extensive use of pulsed-wire anemometry allowed measurements of all the Reynolds stresses throughout the flow, along with some velocity autocorrelations and integral timescale data. The latter help to substantiate the results of other workers obtained in separated flows of related geometry, particularly in the identification of a very low-frequency motion with a timescale much longer than that associated with the large eddies in the shear layer. Wall-skin-friction measurements are consistent with the few similar data previously published and indicate that the thin boundary layer developing beneath the separated region has some 'laminar-like' features.

The Reynolds-stress measurements demonstrate that the turbulence structure of the separated shear layer differs from that of a plane mixing layer between two streams in a number of ways. In particular, the normal stresses all rise monotonically as reattachment is approached, are always considerably higher than the plane layer values and develop in quite different ways. Flow similarity is not a useful concept. A major conclusion is that any effects of stabilizing streamline curvature are weak compared with the effects of the re-entrainment at the low-velocity edge of the shear layer of turbulent fluid returned around reattachment. It is argued that the general features of the flow are likely to be similar to those that occur in a wide range of complex turbulent flows dominated by a shear layer bounding a large-scale recirculating region.

1. Introduction

There have been many quite detailed studies of separated turbulent flows behind steps, fences and similar obstacles. The earliest experiments generally concentrated on the relaxing flow downstream of the separated region (e.g. Tillman 1945; Mueller & Robertson 1963; Plate 1971; Bradshaw & Wong 1972; Castro 1979) although some authors attempted measurements in the recirculating flow (e.g. Arie & Rouse 1956; Good & Joubert 1968). Without really appropriate instrumentation, however, the latter is exceedingly difficult and only recently, with the advent of pulsed-hot-wire and laser anemometry techniques, has there been more effort directed towards the

† Present address: Department of Chemical Engineering, Imperial College of Science and Technology, London SW7 2AZ, UK.

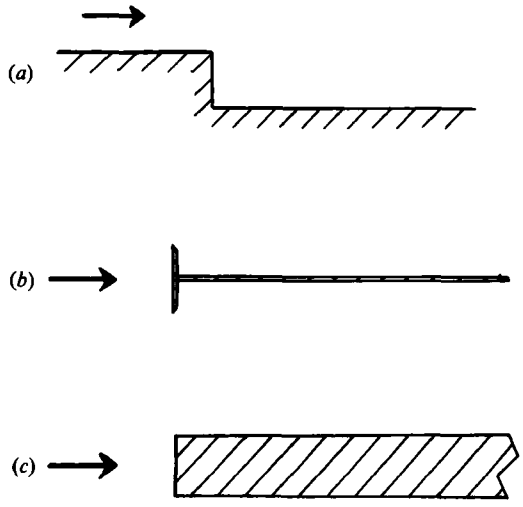

FIGURE 1. Typical geometries for recirculating flows.

nature of the separated region itself. Flow down a rearward-facing step (figure 1*a*) has almost become a classic case – it was selected as one of the two central test cases for comparison with numerical prediction methods at the 1980/1 Stanford Conference on Complex Turbulent Flows (Kline, Cantwell & Lilley 1982) – but even for this geometry the majority of the experimental data have been obtained with standard hot-wire anemometry and pressure probes. These techniques are generally recognized to be inadequate in such flows. Adams, Johnston & Eaton (1984) present a fairly complete list of the 25 or so published studies of rearward-facing-step flows but in only a handful of these were laser or pulsed-wire anemometry techniques used. Notable amongst the latter are the studies of Driver & Seegmiller (1982), Pronchick & Kline (1983) (lasers) and Eaton & Johnson (1980), Westphal, Eaton & Johnston (1984) (pulsed wires).

Other geometries have received much less attention. The simple case of a normal two-dimensional flat plate with a long central splitter plate in its wake (figure 1*b*), first studied by Arie & Rouse (1956), is quite attractive as a typical recirculating flow. Unless the Reynolds number is very low the strong favourable pressure gradient towards the edge of the plate will ensure a thin, laminar boundary layer at separation with transition occurring soon afterwards. Consequently the influence of the ratio of the boundary-layer thickness to the plate height will not be as important a parameter as it seems to be in step flows. Further, although the flow is harder to predict than step flows, if only because the numerical problems are more severe, it is much more typical of bluff-body flows and therefore attractive as a 'test' case. Ruderich & Fernholz (1986) have recently reported a fairly detailed investigation of such a flow, using hot-wire and pulsed-wire anemometry.

A similar geometry, the forward-facing blunt plate (figure 1*c*) has also received some attention, notably from Hillier and co-workers (Cherry, Hillier & Latour 1983, 1984) and Kiya & Sasaki (1983, 1985). The latter authors used split-film anemometry, which may be more reliable than more standard instrumentation. There are various common features of all these flows. One of the more subtle is the fairly recent finding that the flow contains a surprisingly low-frequency energy component. This motion

has a substantially longer timescale than that of the largest eddies in the separated shear layer itself and seems to be linked to a quasi-periodic 'bursting' of the whole bubble. Detailed explanations remain controversial but the phenomenon itself has been clearly seen in the step flows (Eaton & Johnston 1980, 1982), blunt-plate flows (Cherry *et al.* 1984; Kiya & Sasaki 1983) and flows over surface-mounted fences (Castro 1981).

A more obvious general feature is that each flow is characterized by a substantial backflow region, bounded on its lower side by a wall and on its upper side by a turbulent shear layer. This shear layer reattaches at some (mean) distance downstream, set largely by the obstacle geometry and the entrainment needs of the shear layer itself. Although there have been attempts to view the shear-layer development and reattachment as a boundary-layer problem (Green 1966) most authors consider the separated shear layer as a (distorted) version of the plane mixing layer between two streams. Indeed, some authors have made direct comparisons between, for example, the growth rate and maximum Reynolds stresses of the separated shear layer (some distance upstream of reattachment) and those of the plane mixing layer. However, in the case of backward-step flows, there is a wide variation in published values of the maximum turbulent shear stress occurring in the separated shear layers (see for example Chandrsuda & Bradshaw 1981). Despite this, the statement of Chandrsuda & Bradshaw (1981) that 'the measurements show that the mixing layer bounding a separation bubble with a thin initial laminar boundary layer is *not* greatly different from a plane mixing layer' probably represents a consensus view. There is no doubt, however, that the accuracy of the majority of the data on which such views are based is doubtful. Strictly, the ordinary plane mixing layer is a separated shear layer, but in this paper the latter term refers solely to a mixing layer bounding a region of highly turbulent reversed flow.

The data of Ruderich & Fernholz (1986) and Kiya & Sasaki (1983) indicate lower shear-layer growth rates but higher turbulent stresses than those in a plane mixing layer; such data are not really consistent with the idea that the separated shear layer is even self-similar, let alone closely like the self-preserving plane mixing layer. However, it seems that definitive statements regarding the nature of time-averaged quantities throughout separated shear layers will not be possible until a larger body of more accurate data becomes available. Paradoxically, studies of the unsteady nature of the flow have been rather more fruitful, since much can be gleaned by correlation and spectral measurements of surface pressures and of velocities on the outer edge of the shear layer, where turbulent intensities are low enough to make standard anemometry viable. It is evident that whilst some features of the large-scale eddy structures are similar to those occurring in the plane mixing layer, others are certainly not (Cherry *et al.* 1984; Kiya & Sasaki 1985).

The purpose of this paper is to present a fairly comprehensive set of measurements obtained throughout a separated shear layer, to compare them with standard data for the two-dimensional plane mixing layer and to comment on the causes of the major differences between the two shear layers. For convenience we have used as 'standard' plane layer data the results of Castro (1973) which Rodi (1975) states are representative. Comparisons with other recently published data are included where appropriate. The work forms part of a continuing programme of research on turbulent separated flows. A companion paper will present the results of a concurrent investigation of the effects of free-stream turbulence on the flow discussed here. Pulsed-wire anemometry has been used extensively and the data includes measure-

ments of all the Reynolds stresses, mean and fluctuating wall shear stress, velocity autocorrelations and timescales. In order to ensure a reasonably large-scale separation region we have used the flat-plate geometry shown in figure 1(*b*).

Section 2 describes the experimental arrangements and in §3 the basic results are presented and discussed. Section 4 describes the behaviour of some of the turbulence structural parameters relevant to calculation methods and includes a presentation and discussion of the autocorrelations and integral timescales. The conclusions are indicated in §5 where it is emphasized that the separated shear layer differs from the plane mixing layer in a number of important respects. It is our contention that this will be true, to a greater or lesser extent, for *all* separated shear layers.

2. Experimental arrangements

2.1. *The basic flow*

Figure 2 shows the overall set-up of the 6 mm thick flat plate spanning the shorter width of the 0.77×0.62 m working section of the blow-down low-speed wind tunnel in the Mechanical Engineering Department, University of Surrey. The plate height, $2H$, was 50 mm and its edges were bevelled at 30° to the front face, eliminating any possibility of reattachment onto the plate itself. A splitter plate, 3 mm thick, $35H$ long and fitted with instrumentation ports was located behind the normal plate and on the symmetry axis. The mean velocity in the empty working section was uniform to within $\pm\frac{1}{2}\%$, with a longitudinal turbulent intensity of less than 0.25 %.

There are a number of parameters that affect the distance to the mean reattachment point x_R, but in the absence of free-stream turbulence and strong three-dimensional effects the most dominant is the blockage ratio, defined here by h_f/D, where h_f is the height of the fence tip above the surface of the splitter plate (23.9 mm) and D is the tunnel half-height (385 mm). Smits (1982) has shown how x_R/h_f varies with h_f/D and the present value, obtained by oil flow visualization, by twin-tube pressure gauge (Castro & Fackrell 1978) and by the pulsed-wire skin-friction probe (see below) is compared with his data and that of Ruderich & Fernholz (1986) (hereinafter denoted by RF) in figure 3. $2W$ is the spanwise width of the tunnel or the distance between side plates, if fitted. In the present case side plates, extending upstream of and above the splitter plate by about $10h_f$ and positioned $19h_f$ apart, were found to improve the two-dimensionality of the flow. Without them x_R was a little lower than the value ($x_R/h_f = 19.2$) plotted in figure 3. An earlier experiment in a larger wind tunnel in the Department of Civil Engineering, University of Surrey, gave a further result, also plotted in figure 3. This is noticeably below the rest of the data, but it was found that the reattachment line was substantially more curved in this case even though the spanwise aspect ratio was 50 % higher. Figure 4 shows the spanwise variation of x_R plotted as a function of z/W; it seems clear that end plates can effect an improvement. Our oil flow visualizations showed features generally similar to those described by RF; it is doubtful whether the vortex structures in an endwall–fence–splitter plate junction (see RF, figures 4 and 6) could ever be entirely suppressed and they must always have more effect on the flow than in the case of the back-step geometry (Brederode 1975), but the evidence suggests that endplates can at least weaken their influence, presumably because the upstream sidewall boundary layer is then relatively thin. From the x_R spanwise distributions and also some spanwise measurements of mean velocity within the shear layer it was evident that for the present purposes the flow was adequately two-dimensional.

Top-to-bottom flow symmetry was checked by measuring x_R on the bottom surface

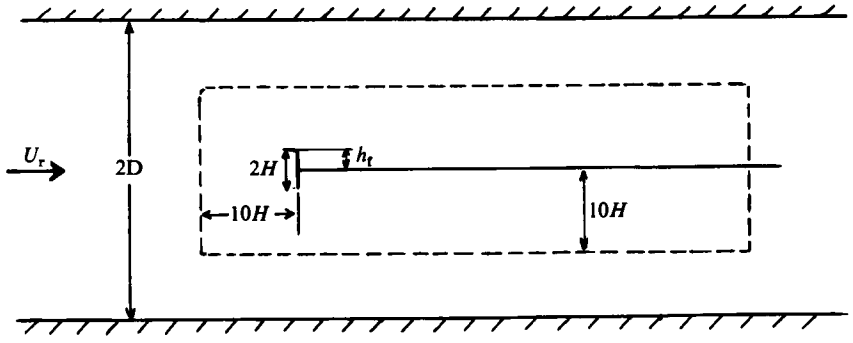

FIGURE 2. Experimental arrangement; not to scale. ——, sideplate boundaries.

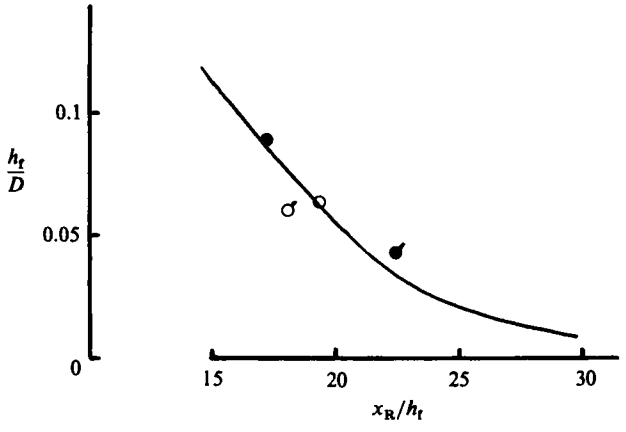

FIGURE 3. Distance to mean reattachment x_R. ——, Smits (1982); source: ●, RF, $2W/h_f = 40$; ◐, RF, 20; ◯, present, 28, in larger tunnel; ○, present, 19.

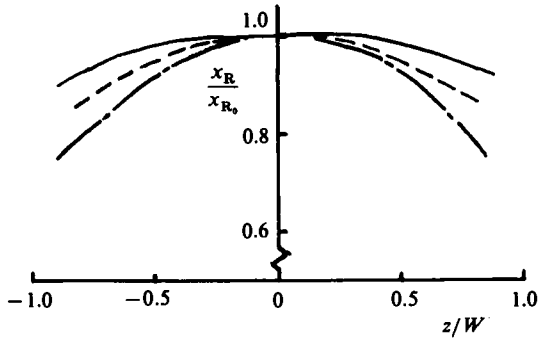

FIGURE 4. Spanwise reattachment lines. ——, RF (no sideplates). Present: ——, $W/h_f = 19$ (with sideplates); ——, $W/h_f = 28$ (no sideplates, larger tunnel).

and by comparing surface pressures on the front of the flat plate itself. The former was within 4 % of x_R on the top surface, whilst the plate front-face pressure coefficient at $y/H = 0.77$, defined as $C_p = (p_s - p_r)/\frac{1}{2}\rho U_r^2$, where suffix r refers to conditions at the reference location about $40h_f$ upstream, was within ± 1.5 % of 0.70 on both sides of the symmetry plane.

2.2. *Instrumentation*

Some initial work, largely associated with setting up the flow and checking spanwise and top-to-bottom symmetry, was undertaken using standard single and crossed hot-wire anemometry. However, data obtained in this way will not be presented since generally it is our belief that its accuracy is not as high as that of the pulsed-wire data. This is almost self-evident in regions where there is a significant probability that the instantaneous flow is in the reverse direction (or at an angle greater than 45° to the x-direction in the case of 45° crossed wires). On the high-velocity side of the shear layer where the turbulent intensities are lower, the data from both instruments agreed to within the experimental uncertainties of either, except at the extreme outer edge of the flow. Pulsed-wire anemometry is unable to make accurate *turbulence* measurements for local intensities less than 2 %. It is worth discussing the reasons for our general confidence in the pulsed-wire measurements, particularly as this is one of the first studies in which the technique has been used to obtain a large quantity of Reynolds-stress data.

Considerable effort was devoted to ensuring adequate directional characteristics of the pulsed-wire probes. The standard probe (see, for example, Bradbury & Castro 1971) has the two sensor wires in the plane normal to the axis of the pulsed wire. The yaw response of such a probe has been shown to approximate $U_\theta = U_0 \cos\theta(1+\epsilon\tan\theta)$, where ϵ is a small parameter, typically about 0.1. For velocity vectors inclined at θ to the probe, thermal diffusion was thought to be responsible for the slight reduction in heat-tracer flight time below the expected value based on the result at $\theta = 0$ (Bradbury & Castro 1971; Bradbury 1976). However, more recent work has shown that this effect is smaller than had been thought. Figure 5 shows results of a detailed yaw-response calibration, from which it is clear that the viscous wake of the upstream sensor wire has a measurable effect and, since the normalizing velocity is usually taken as that measured at $\theta = 0$, leads to measured velocities at non-zero angles apparently exceeding $U_0 \cos\theta$. Figure 5 shows the yaw response of a new type of probe, in which the sensor wires lie in a plane at about 30° to the pulsed-wire axis. The viscous wake is hardly noticeable (since it occurs where $\partial U/\partial\theta$ is relatively large) and the data are much closer to the ideal cosine-law response. Similar results have been obtained by Jaroch (1985) who also found that such a probe has an equally satisfactory pitch response.

Now in a detailed study of the errors caused by the probe's imperfect yaw response, Castro & Cheun (1982) showed that even for a standard probe, whose response was limited to $\pm 70°$, errors in the measured shear stress ($\overline{uv}$, obtained by using the probe like a single 45° slanted hot wire) would generally be less than 30 %, and under 10 % once the local turbulent intensity *exceeded* about 30 %. (The local turbulence intensity is defined as u'/U, where u' is the r.m.s. of the fluctuating longitudinal velocity, as usual.) Calculated errors in the normal stress $\overline{v^2}$ were found to be significantly higher although, in practice, measurements of all the stresses in an axisymmetric mixing layer gave results close to those obtained using crossed-wire anemometry, provided the latter were corrected (using Tutu & Chevray's 1975 results) where appropriate to account for high-intensity effects. All the pulsed-wire measurements in the present work were undertaken using the new type of probe which not only had $\epsilon = 0$ but, since the wires were rather closer together, responded to velocity vectors up to 80° angles (see figure 5). There is therefore no doubt that the accuracy of the Reynolds-stress measurements must be significantly higher than those quoted above for the

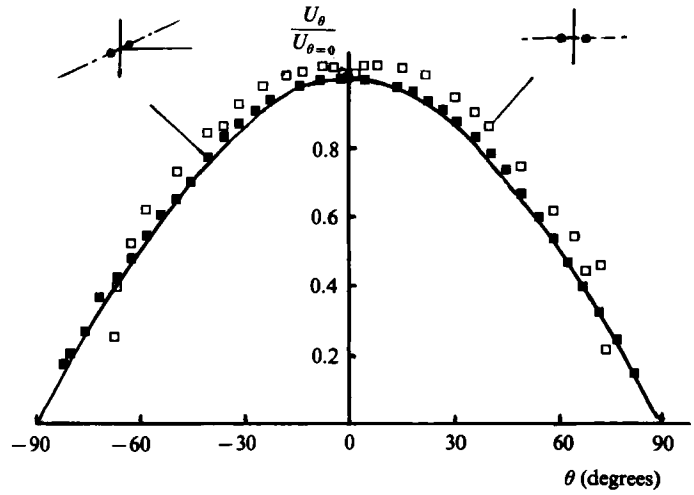

FIGURE 5. Pulsed-wire yaw response. □, standard probe; ■, new probe – sensor wires in a plane at 30° to pulsed wire axis (see insets); ——, cosine.

standard probe. A wider and more detailed discussion of the problems in Reynolds-stress measurements, using any technique, is given elsewhere (Castro 1986).

The probes were calibrated in the free stream against standard Pitot-static tubes, using the relation

$$U = \frac{A}{T} + \frac{B}{T^3},$$

where A and B are constants and T is the heat-tracer flight time. All calibrations and subsequent linearized measurements were performed on-line using Commodore PET computers. In the turbulent flow up to 10000 samples of T were taken at each measurement point, the actual value depending on local intensity, using a sampling rate of 50–100 Hz. Velocity autocorrelations were obtained using the technique described by Castro (1985).

Some kinds of separated flows are very sensitive to disturbances caused by the presence of the probe, but checks showed that in the present case this was not a problem. The geometry ensured a fixed separation point and the diameter of the pulsed-wire-probe support was small (5 mm, narrowing to 2.5 mm for the final 40 mm) compared with the scale of the separated flow ($x_R = 19.2h_f \approx 460$ mm).

Wall-skin-friction measurements were made using a pulsed wall probe (Westphal, Eaton & Johnston 1980; Castro & Dianat 1983) which was calibrated directly against a Preston tube in a well-documented zero-pressure-gradient turbulent boundary layer. Patel's (1965) calibration was used for the Preston-tube data and the pulsed-probe data was well-fitted by a curve of the form

$$\frac{\tau_w}{\rho} = \frac{A}{T} + \frac{B}{T^2} + \frac{C}{T^3},$$

where τ_w is the mean wall shear stress, ρu_τ^2. Since there are substantial fluctuations in τ_w in a turbulent boundary layer it is, in principle, necessary to apply appropriate corrections to the mean time-of-flight values as part of the calibration procedure. A suitable technique was outlined by Westphal *et al.* (1984), but we found that the nonlinearity errors which arise if this is not done were quite small. Ideally, of course,

the probe should be calibrated in a laminar flow; the difficulties associated with this have been discussed by Castro, Dianat & Bradbury (1986). In the present work the probe could be used for instantaneous wall-stress values corresponding to the range $-0.4 < \tau_w/\rho < 0.4$ m^2/s^2.

Wall static pressures were obtained using a 0.5 mm internal diameter hypodermic fixed into a 5 mm plug and connected to a standard capacitance-type transducer. The plug could be moved to any one of a variety of holes drilled on the centreline of the splitter plate, which also served to hold the skin-friction wall probe. Again, the presence of either the skin-friction-probe body and leads or the pressure tubing on the underside of the splitter plate did not noticeably affect the flow on the upper side. Except for the region very close to the wall beneath the separated shear layer, it was found (from measurements of static pressures and x_R) that the flow was sensibly Reynolds-number independent at least in the range $1.5 \times 10^{-4} < Re = 2HU_r/\nu < 5 \times 10^{-4}$. Whilst this is not a very wide range we do not believe that the overall flow at even higher Reynolds numbers would be significantly different. Most of the measurements were made at a free-stream speed of around 7 m/s, giving a nominal Reynolds number based on the plate height of 2.3×10^4.

3. Results and preliminary discussion

3.1. *The mean flow: surface parameters*

The surface static pressure and skin-friction coefficients are plotted in figure 6 against axial distance from the front face of the normal plate normalized by the distance to the mean reattachment point x_R ($19.2h_f$). C_p and C_f are defined by $(p_s - p_r)/\frac{1}{2}\rho U_r^2$ and $\tau_w/\frac{1}{2}\rho U_r^2$, respectively, where p_r and U_r refer to conditions at the reference position. Results for various Reynolds numbers are shown and it is evident that there is a significant trend of decreasing C_f (magnitude) as the Reynolds number rises. The static pressure (and x_R) are much less affected and additional measurements confirmed that further increases in Reynolds number caused barely detectable changes in C_p.

It is possible to renormalize the wall-static-pressure data using a pressure coefficient defined by

$$\tilde{C}_p = \frac{C_p - C_{p\min}}{1 - C_{p\min}}$$

as was first done by Roshko & Lau (1965). This tends to collapse our data with that of other workers (see figure 6*a*), but it is certainly not a universal definition since it has been shown that it does not take account of the effects of strong *imposed* favourable pressure gradient (Devenport 1985).

Now the near-wall region is clearly the only part of the flow likely to be significantly influenced by viscous effects; it is not surprising that there are changes in C_f with Reynolds number even when the latter is large enough to ensure insensitivity in the overall flow. Whilst it is not our purpose here to discuss the near-wall flow in detail, it is instructive to compare the present C_f values with the few data that have been obtained by other workers. This is done in figure 7, where the minimum C_f values, renormalized using the minimum negative velocities occurring above the surface at the appropriate axial location, are plotted against a Reynolds number based on that velocity (U_N) and the distance between the minimum-C_f position and x_R (see inset to figure 7). Ignoring for the moment the unsteady nature of the flow, this can be thought of as the Reynolds number most appropriate for the thin wall boundary layer flowing

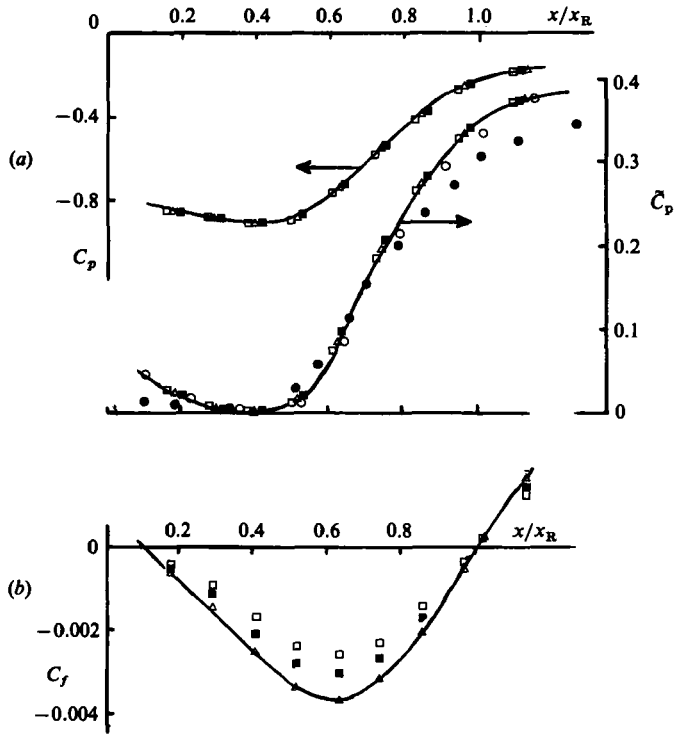

FIGURE 6. Wall-pressure coefficient (*a*) and wall skin-friction coefficient (*b*). △, $Re \times 10^{-4} = 1.49$; ■, 1.81; □, 2.29. Lines added for clarity. Note that (*a*) includes C_p data plotted in the 'Roshko–Lau' normalized coordinates – right-hand axis refers; ●, Roshko & Lau (1965); ○, RF.

upstream from the reattachment point. Some of the data shown are from step-flow experiments (Adams *et al.* 1984; Chandrsuda & Bradshaw 1981; Devenport 1985) and the rest are from RF and the present results at three different Reynolds numbers. Also included are our results obtained with free-stream turbulence, which reduced x_R to $14.4h_t$. A feature of Devenport's experiment is that in one case a substantial centrebody was located downstream of the axisymmetric back-step, inducing a strong favourable pressure gradient on the separated region. It was not possible to measure the appropriate minimum velocity at the location of the minimum C_f, but with a sensible guessed value the date are consistent with the other results.

Not only do the data from all geometries collapse reasonably well, but they also lie on a line having a slope not far from $-\frac{1}{2}$, consistent with the idea that the boundary layer has strong laminar-like features (see Adams *et al.* 1984). The mean velocity data, presented later, suggest that the minimum velocity increases roughly like $(x_R - x)^{1.6}$ in the direction away from the reattachment point (up to roughly the centre of the 'bubble') and figure 7 includes the Falkner–Skan laminar-boundary-layer solution for an imposed favourable pressure gradient appropriate to that 'free-stream' velocity variation. The experimental data are consistent with a rather stronger pressure gradient. It would have been very surprising to see an exact correspondence; throughout this second half of the bubble the instantaneous wall friction could have either sign. The data of Westphal *et al.* (1984) and RF show that nowhere in the reversed-flow region does the reverse-flow intermittency, defined as the fraction of time during which the wall flow is upstream, exceed 95 %. Further, recent flow

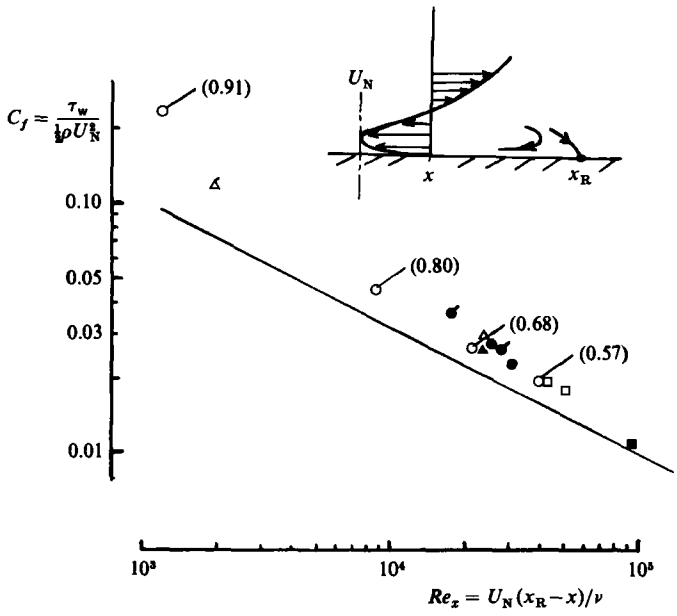

FIGURE 7. Wall friction in second half of the reversed-flow region. Bracketed values are x/x_R for the present experiment at $Re = 23000$. Other points are *maximum* values in the 'bubble'. △, Devenport (1985), axisymmetric step; ⧋, ditto, with centrebody; ■, Chandrsuda & Bradshaw (1981), step; ▲, Adams *et al.* (1985), step; ●, RF; ◐, present, with free-stream turbulence. The solid line is the Falkner–Skan laminar-boundary-layer result.

visualization of the near-wall region suggests that a description of it as being essentially laminar is far too simplistic (H. H. Fernholz, private communication). Nonetheless, the boundary layer must be strongly influenced by viscous effects and so behave in some ways like other viscous phenomena – hence the term 'laminar-like'.

What does seem clear is that the particular flow geometry, at least in the range so far covered, has little influence on the correlation between C_f and Reynolds number when these parameters are normalized as in figure 7. Further discussion concerning the features of the near-wall flow is given by Adams *et al.* (1985) and by Devenport (1985), who both made detailed measurements close to the wall.

3.2. *The mean flow: velocity field*

The bulk of the mean and turbulence data were obtained from y-direction traverses of the pulsed-wire anemometer from $y/H = 0.25$ to 4.0 at axial stations nominally $2H$ apart, between $x/H = 2$ and 24. There is therefore a considerable quantity of data and it would not be appropriate to present it all. Throughout this and all following sections attention is concentrated on appropriately normalized results at just a few axial stations (generally $x/x_R = 0.35$, 0.68, 1.02 and 1.36) along with the variation of quantities along a suitably defined shear-layer 'centreline'.

Figure 8 presents typical axial mean velocity profiles at $x/x_R = 0.35$, 0.68, 1.02, and 1.36 ($x_R = 19.2h_f$) and figure 9 shows streamlines, obtained by integrations of all the velocity profiles outward from the wall. Stream-function values are defined by

$$\psi = \int_0^y \left(\frac{U}{U_r}\right) \mathrm{d}y,$$

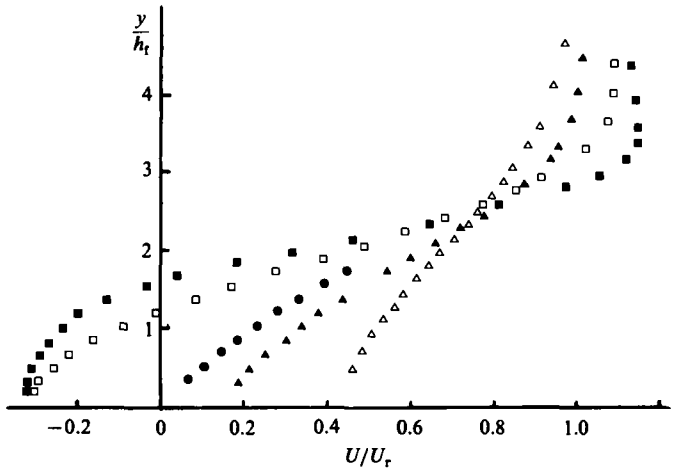

FIGURE 8. Mean velocity profiles. ■, $x/x_R = 0.35$; □, 0.68; ●, 0.96; ▲, 1.02; △, 1.35.

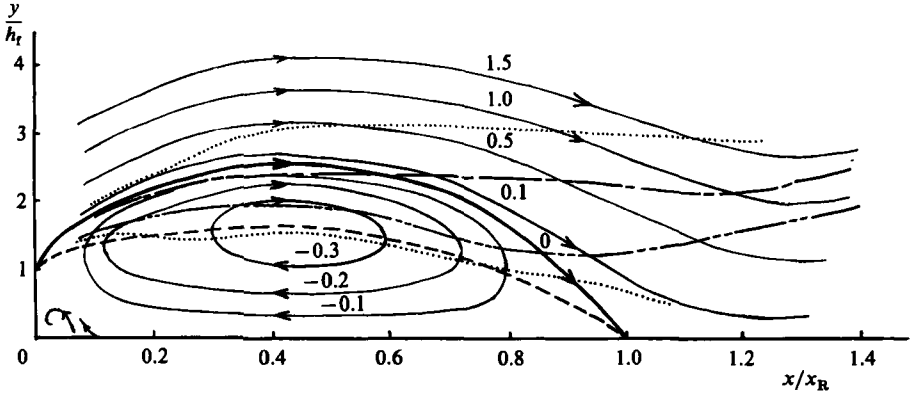

FIGURE 9. Mean streamlines. Figures refer to ψ-values. ——, locus of $U = 0$; ——, locus of $\eta = 0$; – – – – –, locus of maximum turbulence energy; ·····, locus of $U/\Delta U = 0.1$ and 0.9.

where y-values are here (and hereafter) normalized by h_t. Included in the figure are the lines along which $U = 0$, $\psi = 0$, $\eta = 0$ (see later) and u^2 is a maximum.

The pulsed-wire anemometer traverses undertaken at probe angles of $\pm 45°$ in order to deduce $\overline{v^2}$ and $\overline{uv}$ also resulted in measurements of the vertical (V) component of mean velocity. Some of the raw data are shown in figure 10, where they are compared with data obtained by solving the continuity equation using the measured U-component results. It is satisfying that the results are generally consistent to within about $\pm 2\,\%$ of U_r, which is about the same order of accuracy as that expected from crossed hot-wire anemometry in regions where the latter could sensibly be used.

The growth of the shear layer is commonly measured in terms of the increase in its vorticity thickness Λ defined by

$$\Lambda = 1 \Big/ \left| \frac{\mathrm{d}(U/U_r)}{\mathrm{d}y} \right|_{\max}.$$

This is shown in figure 11, normalized by x_R and plotted against x/x_R. Many authors have suggested that their measurements imply a roughly linear growth rate but

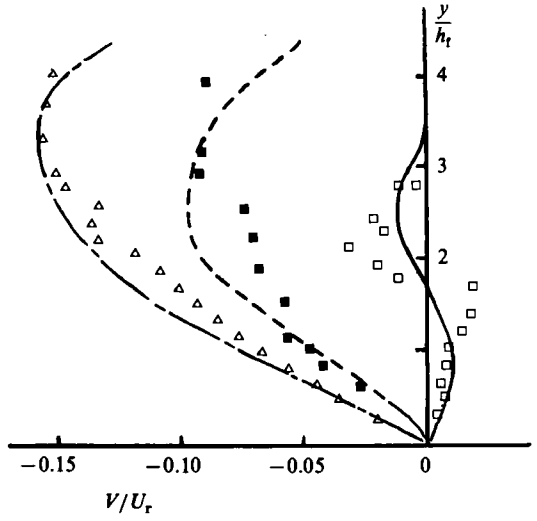

FIGURE 10. Vertical mean velocity at □, $x/x_R = 0.46$; ■, 0.68; △, 1.02. Lines are from integration of the continuity equation, using measured longitudinal velocity data.

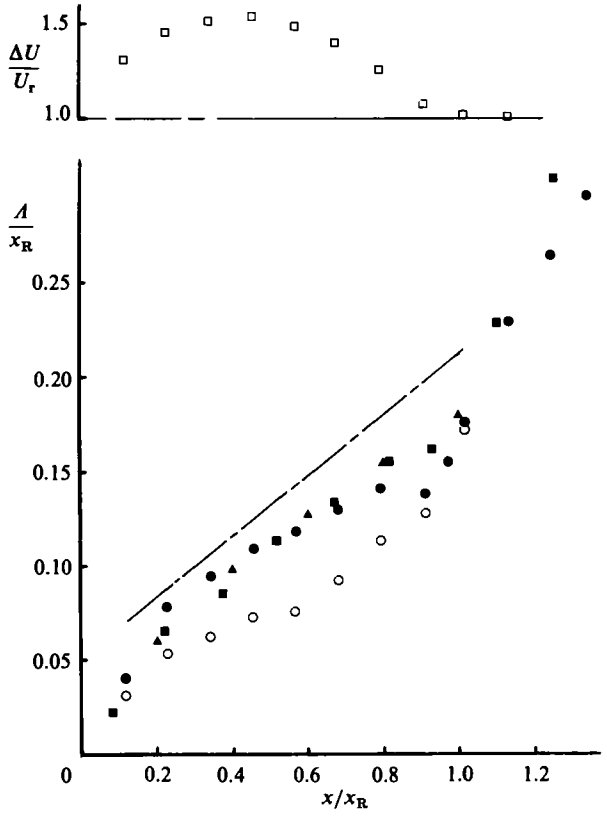

FIGURE 11. Growth of the vorticity thickness. ○, present work, Λ based on U_r; ●, present work, Λ based on ΔU; ▲, Kiya *et al.* (1982) (blunt plate); ■, RF. ——, plane mixing layer (arbitrary virtual origin); □, $\Delta U/U_r$, present work.

almost invariably this is deduced from rather fewer profiles than in the present work. Further, as has been previously pointed out (e.g. Bradshaw & Wong 1972; RF) any comparison between Λ and the plane-mixing-layer value should arguably take into account the fact that the actual velocity difference across the separated shear layer is markedly higher than U_r. Figure 11 includes values of Λ in which ΔU, the actual velocity difference $(U_{max} - U_{min})$, is used as the reference velocity, compared with results from RF and Kiya *et al.* (1982) for the blunt-plate geometry; these authors also used ΔU as the reference velocity. The variation of $\Delta U/U_r$ in the present case is shown in the figure.

It is clear that the present data are not really consistent with a linear increase in Λ and in all cases the results tend to suggest a slowly decreasing growth rate up to reattachment followed by a relatively rapid increase. The initial shear-layer growth rate is significantly higher than the plane-mixing-layer value; this conclusion would not be altered by measuring x along the path of the shear layer. Use of a Λ based on velocities measured in the direction of any appropriate shear-layer centreline would also not significantly affect the trends in figure 11.

Other similar (unpublished) experiments in our laboratory also indicate a gradually reducing growth rate up to reattachment for cases in which the fence (or a block) is surface mounted within a turbulent boundary layer. Further discussion is given later, but it is worth pointing out here that there is no reason why, in this complex flow, the shear layer *should* grow linearly, whatever parameters are used to define Λ.

3.3. *The shear-layer direction*

It is obvious from the streamline plot in figure 9 that the local direction of the shear layer changes significantly as the flow develops. Consequently it could be argued that the Reynolds stresses should be referred to some appropriate local axes aligned with the mean flow, rather than (x, y)-axes. We can define the shear-layer centreline, by analogy with the plane mixing layer, as the line along which the mean velocity is $(0.67\Delta U + U_{min})$, where U_{min} is the minimum velocity on the low-speed side of the layer; $U_{min} < 0$ for $x < x_R$. Figure 9 includes the locus of this line, shown as $\eta = 0$. η is defined by $\eta = -(y - y_c)/\Lambda$, where y_c is the height of the '0.67-velocity' line and the negative sign ensures that $\eta < 0$ on the high-velocity side of the mixing layer, in common with the usual plane mixing layer similarity variable. Figure 12 shows the mean flow direction (β_1) on this line.

Other definitions of the shear-layer direction are possible, of course. One obvious one is the actual direction β_2 of the $\eta = 0$ locus; others could include the direction the flow along the line of maximum $\overline{q^2}$, (β_3) or the direction β_4 of the streamline defined by $\psi = 0$. These are compared with β_1 in figure 12 and it is clear that the different definitions of shear-layer direction do not coincide closely over the whole flow. This might suggest that detailed comparisons between the individual turbulent stresses and those in the plane mixing layer may not be too helpful. In a flow where there is no distinctive development direction, discussion should presumably be restricted to the principal stresses and their response to the principal rates of strain. However, in the present case, although there are large changes (at fixed x/x_R) in the local streamline direction on the low-velocity side of the shear layer there *is* a clear qualitative direction of flow development over at least the first two-thirds of the 'bubble' and again of course after the reattachment region. In our discussion of the behaviour of the turbulent stresses we shall use β_1, (which is roughly coincident with β_4 up to $x/x_R = 0.7$) as the local shear-layer direction.

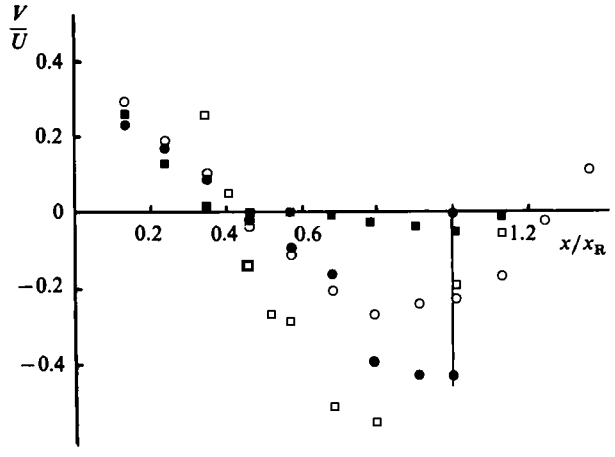

FIGURE 12. $V/U = \tan\beta$, flow direction along: ■, line of maximum $\overline{q^2}$ (β_3); ○, $\eta = 0$ (β_1); ●, $\psi = 0$ (β_4); □, $\eta = 0$ (β_2).

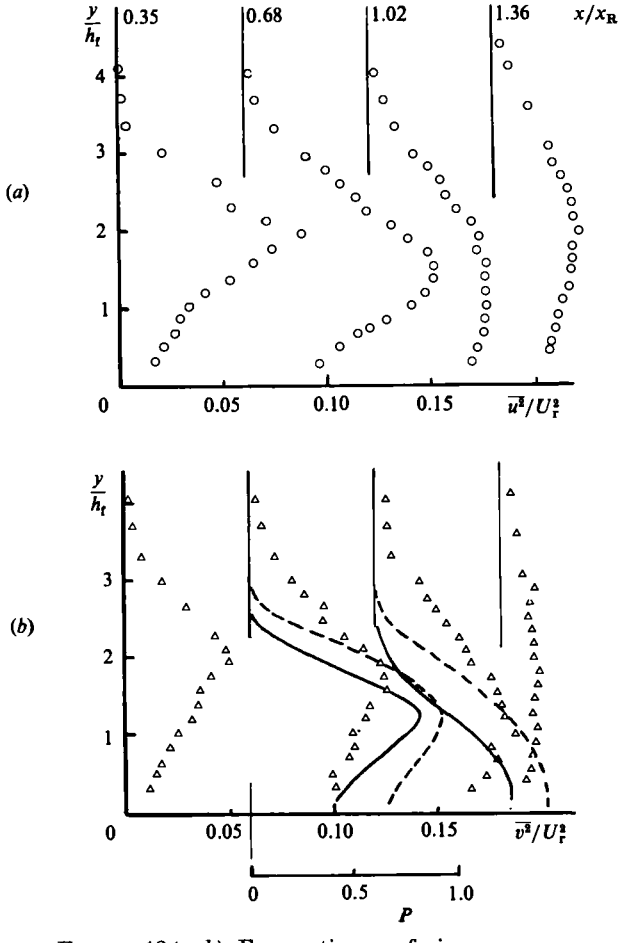

FIGURE 13 (*a*, *b*). For caption see facing page.

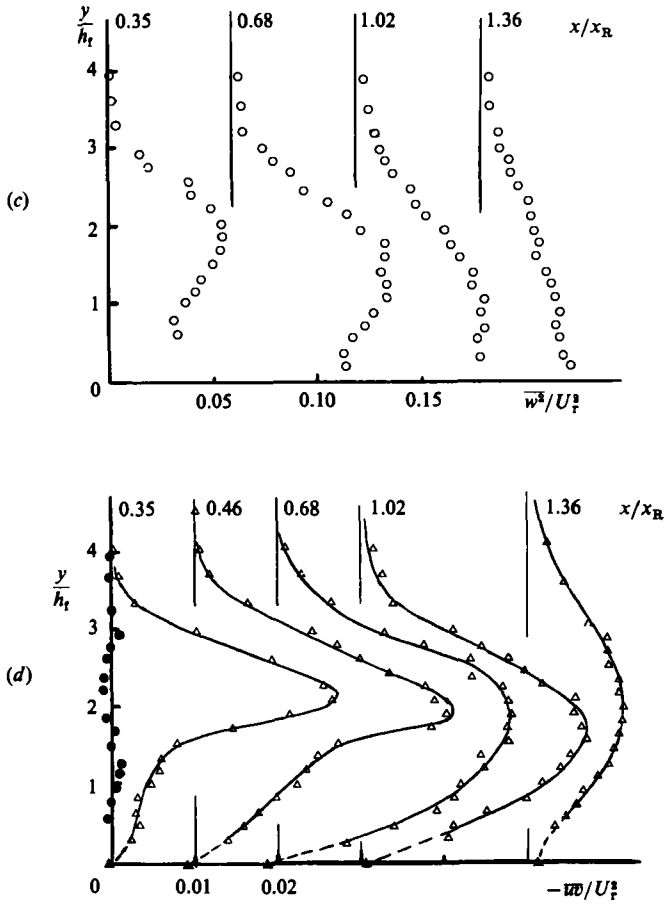

FIGURE 13. Reynolds-stress profiles. (*a*) $\overline{u^2}$; (*b*) $\overline{v^2}$ and probability of velocity vector lying outside a forward-facing cone of included half-angle 45° (——) and 30° (– – –); (*c*) $\overline{w^2}$; (*d*) $\overline{uv}$ and $\overline{uw}$ (●); ▲, $\overline{uv}$ from wall C_f; lines added for clarity.

3.4. *Reynolds stresses*

Figure 13 shows Reynolds-stress profiles (in standard (x, y)-coordinates) at the four axial stations defined earlier. In the case of the shear stress $\overline{uv}/U_\tau^2$ the plots include the wall values measured by the skin-friction probe and an additional profile in the first half of the separated region. The $\overline{uv}$-data measured away from the wall are not inconsistent with the wall values. In the upstream part of the flow ($x/x_R < 0.5$) the $\overline{uv}$-profiles are characterized by a noticeable change in slope on the low-velocity side, consistent with the idea that nearer the wall the turbulent fluid is likely to originate from the reattachment region, rather than being typical of the extreme low-velocity side of an ordinary plane mixing layer. Note that $\overline{uw}$-values are insignificant; this, with the generally low level of scatter in the data, is a further indication of the measurement accuracy.

As a demonstration of the difficulties encountered in using standard instrumentation in such flows, we have used the pulsed-wire measurements to calculate the probability P of the instantaneous velocity vector lying outside forward-facing cones of semi-angle 45°, for conditions at $x/x_R = 0.68$ and 1.02. Gaussian turbulence was

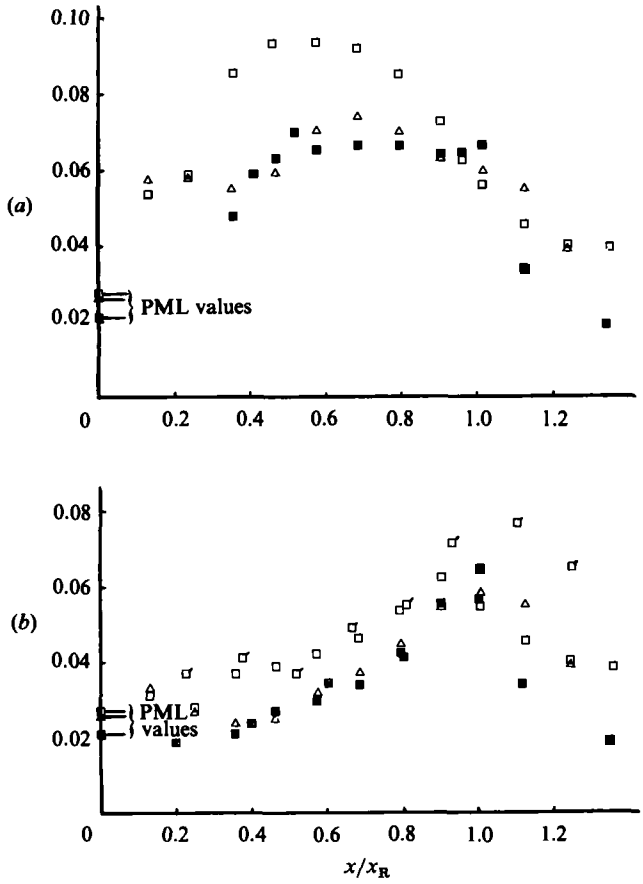

FIGURE 14. Maximum normal Reynolds stresses. □, $\overline{u^2}$; △, $\overline{v^2}$; ■, $\overline{w^2}$. (*a*) Normalized by U_r^2. (*b*) Normalized by $(\Delta U)^2$; ⊠, $\overline{u^2}$, RF; □, $\overline{u^2}$, Kiya & Sasaki (1983). Plane mixing layer (PML) values shown at left.

assumed and values of $\overline{u^2}$, $\overline{v^2}$, $\overline{w^2}$, $\overline{uv}$ and V/U measured by the pulsed-wire anemometer were used in the numerical integration of the joint probability density function (see Castro 1986 for further details). Figure 13(*b*) includes the results, from which it is clear that even if the yaw *and pitch* response of a 45° crossed-wire probe were known accurately for flow inclinations right up to those parallel to the wire axes, rectification effects would make the results seriously in error over a large part of the separated shear layer. At the position of maximum $\overline{u^2}$, for example, P is about 30% for a 45° cone and about 60% for a 30° cone at $x/x_R = 0.68$. Similar results would apply for the mixing layer behind a rearward-facing step and serve to highlight the caution which should be exercised in discussing results obtained using standard hot-wire anemometry. The effects of non-Gaussianity in the turbulence are not likely to be large enough to alter this conclusion. It is worth noting again here that errors in pulsed-wire stress measurements are likely to be at their highest in the *low*-intensity regions of the flow; in practice the measurements in these regions are close to crossed hot-wire results.

Figure 14 shows the variations of the maximum values of the stresses as the flow develops, normalized by U_r^2 (figure 14*a*) and $(\Delta U)^2$ (figure 14*b*). Comparisons with the $\overline{u^2}$ data of RF and Kiya & Sasaki (1983) are included in figure 14(*b*). Whilst the

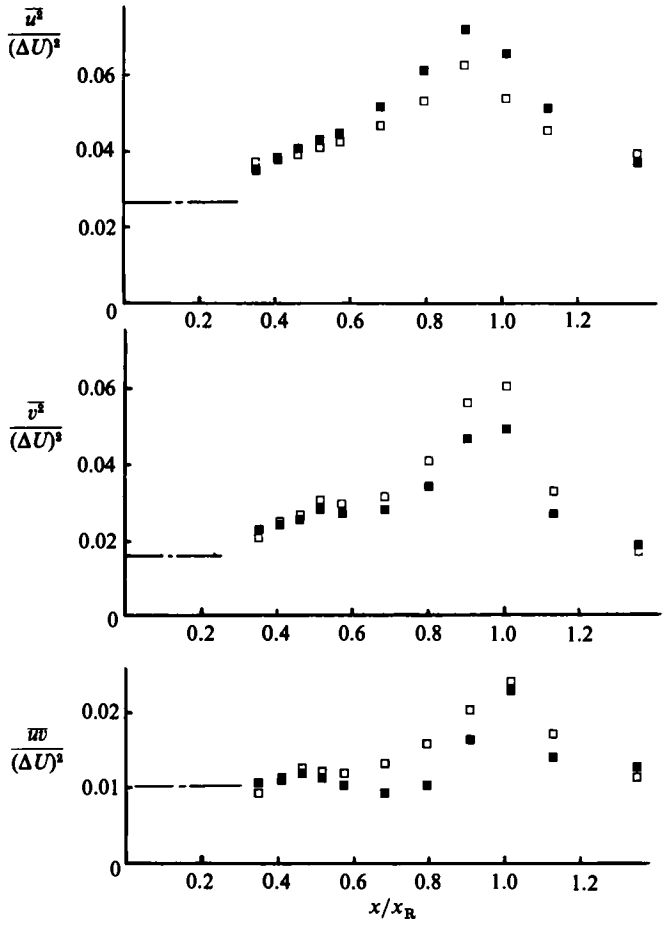

FIGURE 15. Reynolds stress along line of maximum $\overline{u^2}$. Open symbols, (x, y)-coordinates; closed symbols, rotated into the β_1 direction. —·—, plane-mixing-layer values.

pulsed-wire data seem largely consistent, the split-film data of Kiya & Sasaki are rather lower, as might be anticipated. Further, the $\overline{v^2}$, $\overline{w^2}$ and $\overline{uv}$-data of RF (not shown) are all substantially lower than the present results since RF used hot-wire anemometry to obtain their data. Qualitatively, however, the turbulence stresses generally have the behaviour anticipated from previous work in that both normal- and shear-stress levels (see figure 15 for the latter) rise all the way to reattachment if normalized by ΔU^2 and thereafter fall rapidly. In the early part of the flow, the axial stress ($\overline{u^2}$) is larger than the transverse stress ($\overline{v^2}$) by rather more than in the plane mixing layer – values for the latter are shown in the figure. Together with the substantially higher vorticity thickness in this region this may be evidence for 'flapping' of the shear layer. Without such flapping one might expect the strong streamline curvature in the early part of the shear-layer development to *reduce* turbulent stresses and overall growth rates until the effects of motions in the reversed-flow region become important further downstream. We return to this point later.

The Reynolds stresses referred to local axes aligned with the shear-layer direction are compared with the unrotated ones in figure 15. (Here, the values shown are those

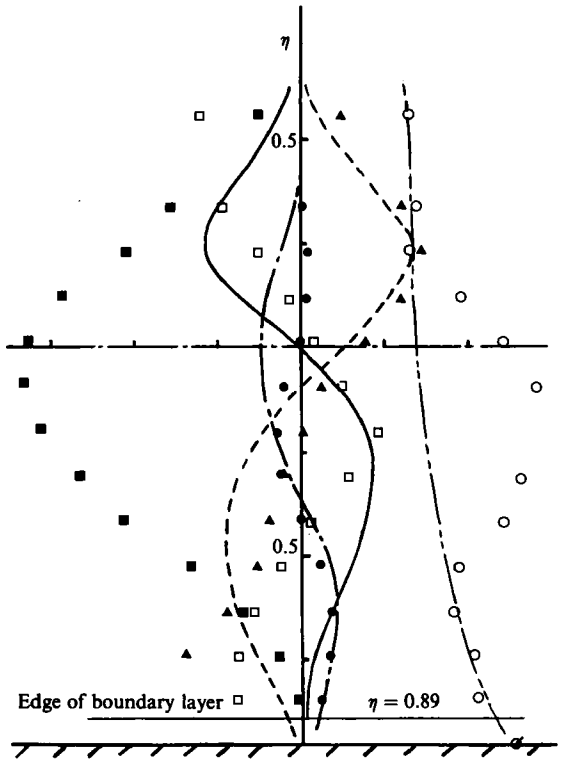

FIGURE 16. Momentum balance at $x/x_R = 0.68$. Lines denote plane mixing layer values. □, ——, $U\,\partial U/\partial x$; ■, – – –, $V\,\partial U/\partial y$; ▲, – · – ·, $\partial\overline{uv}/\partial y$; ●, $\partial\overline{u^2}/\partial x$; ○, $1/\rho(\partial p/\partial x)$ (by difference); ⊘, wall value of $1/\rho(\partial p/\partial x)$. – – – –, underlying monotonic trend in axial pressure gradient (see text).

along the line of maximum $\overline{u^2}$.) Evidently, although β can be in excess of 15° (see figure 12) the overall behaviour of the stresses does not change drastically. The largest proportional effect of the axis rotation is on $\overline{uv}$, which remains roughly constant right up to $x/x_R = 0.8$ when referred to shear-layer axes. $\overline{u^2}$ rises more, whilst $\overline{v^2}$ rises less. It is also worth noting that irrespective of the axes used the fall in $\overline{u^2}$ near reattachment begins slightly earlier than the fall in the other stresses.

3.5. *The mean momentum balance*

The equation expressing conservation of mean momentum in the x-direction is

$$U\frac{\partial U}{\partial x}+V\frac{\partial U}{\partial y}+\frac{\partial\overline{u^2}}{\partial x}+\frac{\partial\overline{uv}}{\partial y}=-\frac{1}{\rho}\frac{\partial p}{\partial x},$$

in which the viscous term has been ignored. The measurements allow calculation of every term except the pressure gradient and even this is available at $y = 0$ and outside the shear layer where it balances the inertial term. Figure 16 shows each term plotted as a function of the similarity variable η, defined earlier, at $x/x_R \approx 0.68$. The terms are each normalized by h_t and $(\Delta U)^2$ and are referred to the usual laboratory (x, y) coordinates. Corresponding results for the plane mixing layer are included and it is evident that the major differences arise from the fact that at this location there is a relatively strong mean V-component. $V(\partial U/\partial y)$ is consequently much larger than it is in the plane mixing layer. Neither $\partial\overline{uv}/\partial y$ nor $\partial\overline{u^2}/\partial x$ return to zero on the

low-velocity side as they do in the plane mixing layer (although the latter must be zero *at* the wall) and it should be emphasized that measurements are not available in the near-wall region below the height at which the axial velocity reaches its minimum (negative) value. This occurs near $\eta = 0.89$, shown in figure 16 as defining the edge of the wall boundary layer. The behaviour of the various terms (other than the pressure gradient) in this near-wall region is uncertain; $\partial\overline{uv}/\partial y$ may not balance $\rho^{-1}\,\partial p/\partial x$ exactly at the wall since there the viscous term will be important.

It is satisfying that the pressure-gradient term, derived by difference from the other terms, extrapolates quite well to the measured wall value and in this sense the results supply some confidence in the general consistency of the data. Note that there is an underlying monotonic variation in the pressure gradient, shown as a dotted line in the figure, from the wall value to the outer-flow-region value, but superimposed on this is a significant rise across the bulk of the shear layer. This is simply a result of the shear layer crossing the coordinate axes (see figure 9), but it does correspond to a real 'hump' in the axial static pressure gradient.

4. Derived results and further discussion

4.1. *Development of the turbulence structure*

We start by comparing the mean velocity and turbulence-stress profiles across the separated shear layer with the classic plane-mixing-layer results. Using the similarity variable η, defined in the last section, the mean velocity and Reynolds-stress profiles at $x/x_R = 0.35$, 0.68, 1.02 and 1.36 are shown in figure 17; plane mixing layer data are included. Results are normalized by ΔU (as is Λ) so collapse of the mean velocity profiles is assured at least in the central part of the layer. In the first part of the 'bubble' the velocity on the low-velocity edge of the layer does not decay as rapidly as it does in the plane mixing layer but further downstream the wall exerts increasing influence so that U then falls more rapidly; after reattachment the decay is again slower.

Figures 17 (*b–e*) emphasize the fact that the turbulent quantities are very different from plane-layer values. The data shown refer to local shear-layer axes but do not differ qualitatively from the corresponding results using (x, y)-coordinates. Further, only in the early part of the flow do the stress profiles have shapes even qualitatively similar to those of the corresponding plane mixing layer profiles and even there the behaviour is different near the wall, particularly in the case of $\overline{uv}$, as noted earlier. At least up to reattachment all the stresses, particularly $\overline{u^2}$, are a little higher than plane mixing layer values on the high-velocity side for $\eta < -0.1$, as might be expected, but for $\eta > -0.1$, there are differences which increase both with x/x_R and with η. Although $\overline{uv}$ is not too far from plane mixing layer values at $x/x_R = 0.35$, the normal stresses are very high in this region. It is also significant that whilst $\overline{uv}$, $\overline{u^2}$ and $\overline{v^2}$ all fall as the wall is approached for $x/x_R > 1$, $\overline{w^2}$ keeps rising until very close to the wall, at which it must reduce to zero of course. Discussion of these results is deferred until later.

In figure 18 the turbulence structure parameters $\overline{uv}/\overline{q^2}$, $\overline{v^2}/\overline{u^2}$ and $\overline{w^2}/\overline{u^2}$ are shown at the four axial stations and compared with plane mixing layer data. These again emphasize the distinct differences between the separated shear layer and the plane mixing layer. At $x/x_R = 0.35$ the stress ratios are close to the fully developed plane mixing layer values on the high-velocity side, but even at this station there are substantial differences for $\eta > -0.1$. Further downstream the differences extend

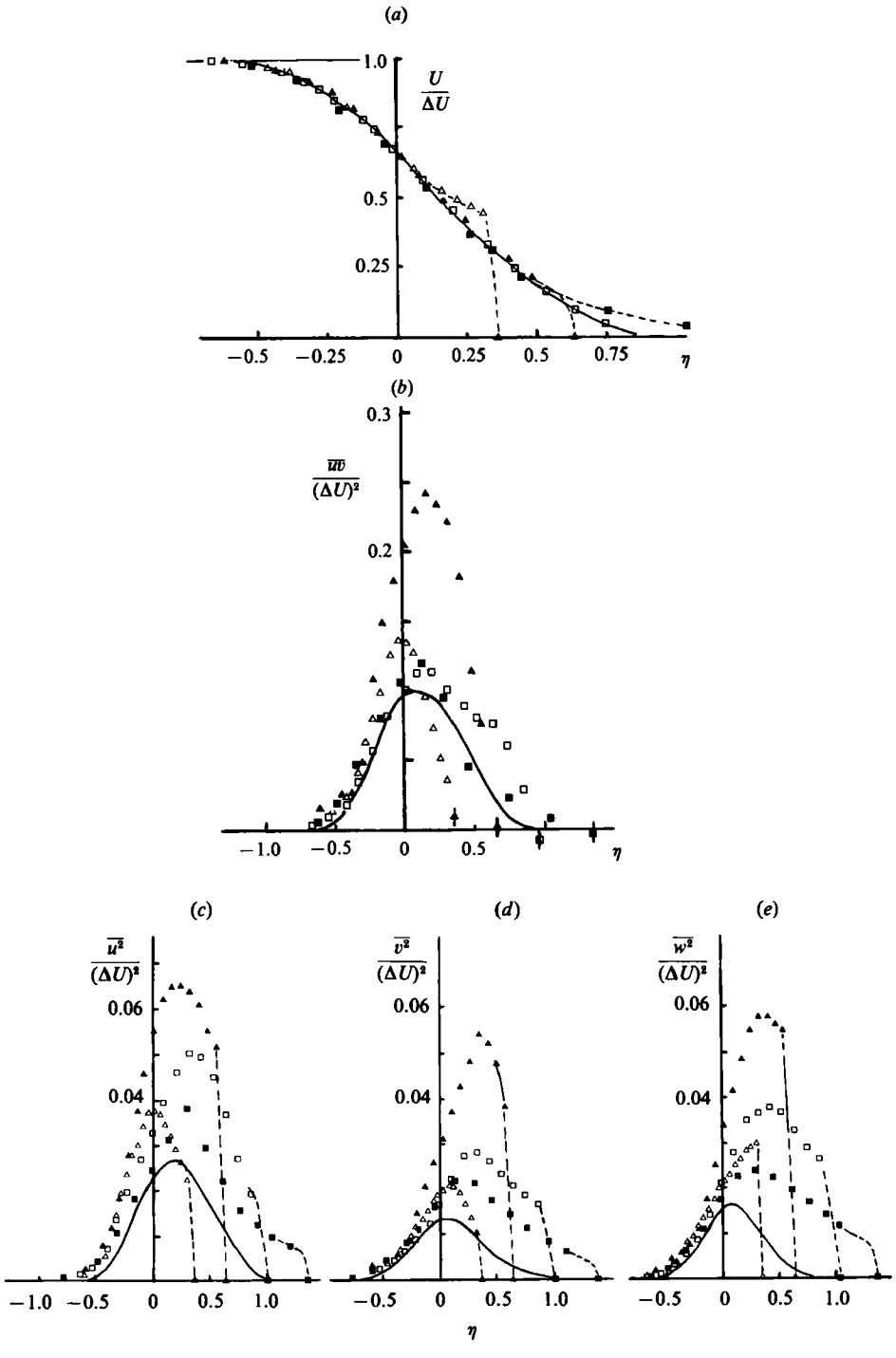

FIGURE 17. Cross-stream profiles. (*a*) mean velocity; (*b*) $\overline{uv}$; (*c*) $\overline{u^2}$; (*d*) $\overline{v^2}$; (*e*) $\overline{w^2}$. ■, $x/x_R = 0.35$; □, 0.68; ▲, 1.02; △, 1.36. ——, plane-mixing-layer values. Wall locations are also indicated.

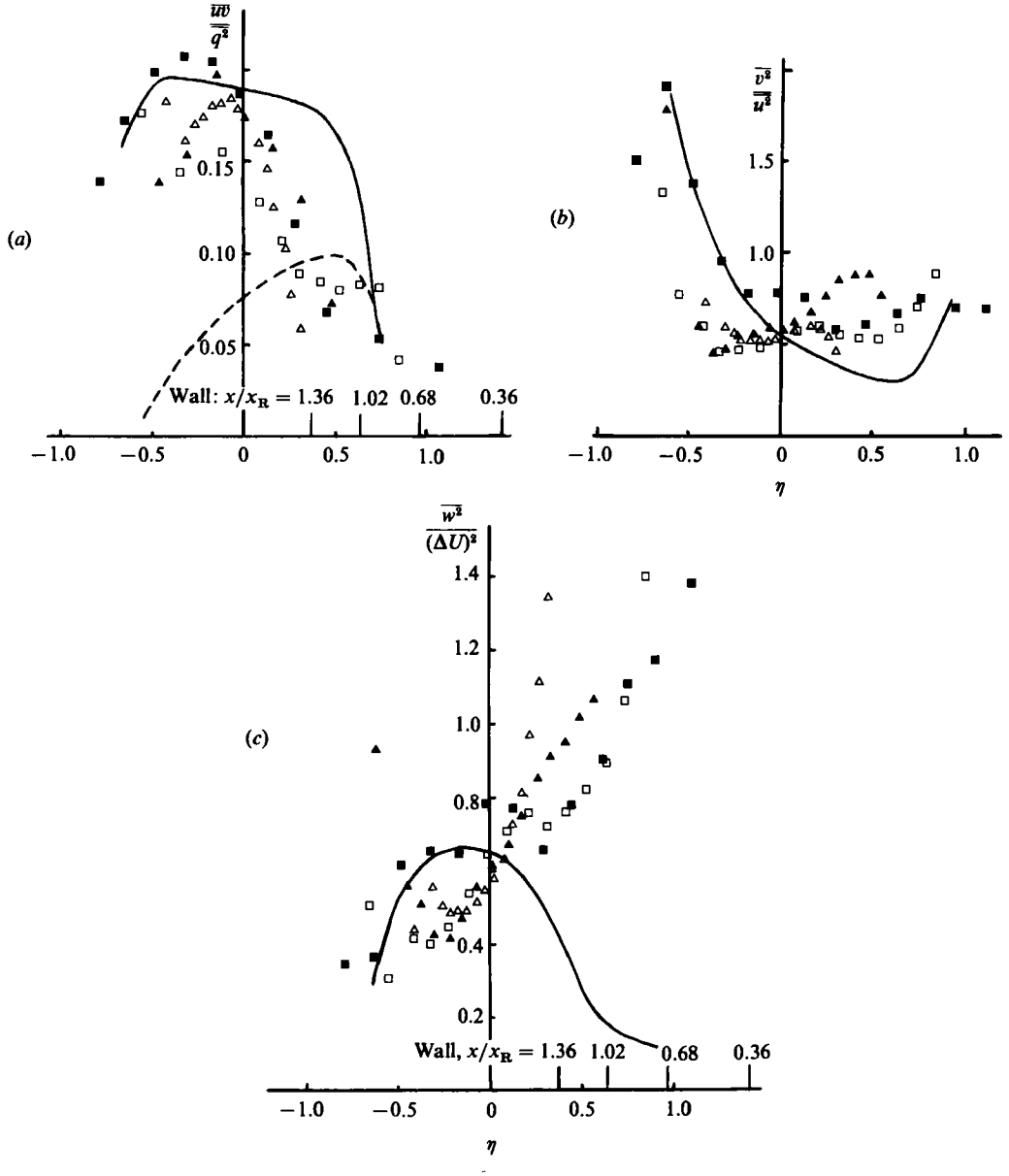

FIGURE 18. Turbulence structure functions (*a*) $\overline{uv}/\overline{q^2}$; (*b*) $\overline{v^2}/\overline{u^2}$; (*c*) $\overline{w^2}/\overline{u^2}$. Legend as in figure 17. η-positions corresponding to the wall location are indicated for each axial station. ----, Castro & Bradshaw (1976) at $A/R = 0.28$.

across the whole layer. It might be possible to achieve collapse of the individual stress profiles by plotting them in similarity form, as RF did, using the local maxima as normalizing values. However, since the levels change so drastically as the flow develops there seems little merit in this procedure.

Figure 18(*a*) shows that the low-velocity side of the shear layer is characterized by a much lower value of $\overline{uv}/\overline{q^2}$ than that in the plane mixing layer, indicating that the shear-stress production is relatively low. This weakening in the 'efficiency' of the turbulence rapidly extends over the whole flow as x increases. There are perhaps two

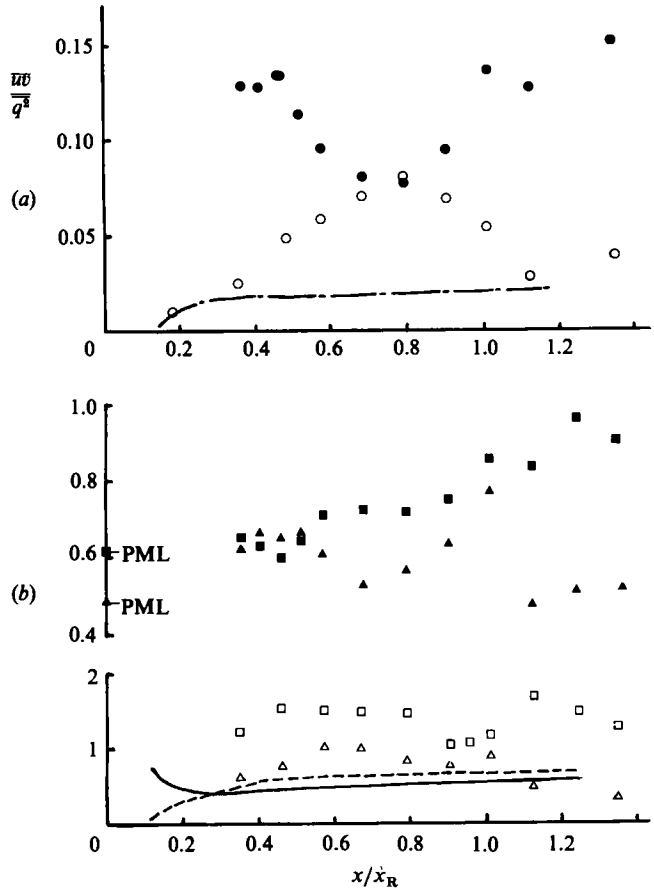

FIGURE 19. Structure functions along the centreline (solid symbols) and along $y/h_f = 0.27$ (open symbols). Lines are for plane mixing layer at the same distance from $\eta = 0$ as the y/h_f point. (*a*) $\overline{uv}/\overline{q^2}$, ——; (*b*) ——, □, ■, $\overline{w^2}/\overline{u^2}$; ——, △, ▲, $\overline{v^2}/\overline{u^2}$.

major possible reasons for this. First, the curvature of the shear layer is in a stabilizing sense from separation virtually all the way to reattachment. In fact, the locus of the separating streamline ($\psi = 0$ on figure 9) roughly forms a circular arc with a radius R of about $25h_f$ between $0.1 < x/x_R < 0.9$. This implies values of the curvature parameter Λ/R ranging from about 0.02 at $x/x_R = 0.1$ to about 0.12 at $x/x_R = 0.9$. These values are comparable with those in the curved-mixing-layer experiment of Castro & Bradshaw (1976). Now in that experiment all the turbulent stresses were reduced by the imposed extra rate of strain whereas in the present flow they increase (figures 14 and 15). Despite this, the behaviour of $\overline{uv}/\overline{q^2}$ is quite similar. Figure 19(*a*) shows how this parameter varies with x/x_R (along the line of maximum $\overline{u^2}$); by $x/x_R = 0.8$ it is reduced by a factor of two from the plane-mixing-layer value. Although this result is reminiscent of the behaviour found by Castro & Bradshaw we do not believe that there are any really useful similarities between the two flows. In figure 18(*a*) the cross-stream variation of $\overline{uv}/\overline{q^2}$ in the former experiment is shown for comparison for the station where the curvature parameter Λ/R was near its maximum (about 0.28). It is clear that the behaviour is quite different from that in the present case. Shear-stress levels were reduced far more, compared with reductions

in turbulence energy, on the high-velocity side of the layer whereas in the present case the largest reductions occur on the low-velocity side.

A second and more likely cause of the general reductions in $\overline{uv}/\overline{q^2}$ in the present case is simply that the separated shear layer entrains highly turbulent fluid on its low-velocity side. Although this fluid presumably has significant shear stress (recall the slow decay of $\overline{uv}$ as the wall is approached for $x/x_R < 0.5$, see §3.4) this will generally be uncorrelated with the stress in the local turbulent fluid of the shear layer. Consequently, whilst the turbulence energy rises substantially, the shear stress does not. This 'lower boundary condition' on the separated shear layer seems much more significant than the stabilizing effects of the mean flow curvature.

A further complicating factor could be associated with the initial conditions of the separated shear layer. Bradshaw (1967) has shown that full mixing-layer development probably does not occur much before a downstream distance equivalent to 1000 momentum thicknesses of the initial boundary layer, if the latter is laminar. Upstream of this point all the Reynolds stresses are somewhat higher than their fully developed values. The momentum thickness of the separating boundary layer in the present case can be estimated to be about $0.002h_f$, so this criterion might suggest that in the absence of other effects the stresses upstream of $x/h_f = 2$ ($x/x_R = 0.1$) would be high. Stabilizing curvature might delay the approach to transition and full development but, again, it seems more likely that even in this region close to the normal plate the effects of the entrainment of highly turbulent fluid will be dominant. Certainly the general levels of the stresses and structure functions along the line of maximum $\overline{u^2}$ in the early part of the flow do not seem unreasonably different from fully developed plane mixing layer values (figures 14 and 19). Cherry *et al.* (1984), in their experiments on the blunt-plate geometry, found no evidence of persistent transitional effects.

Whilst $\overline{uv}/\overline{q^2}$ is generally reduced over the whole of the shear layer, both $\overline{v^2}/\overline{u^2}$ (figure 18*b*) and $\overline{w^2}/\overline{u^2}$ (figure 18*c*) are significantly higher than plane-mixing-layer values on the low-velocity side. In the case of $\overline{w^2}/\overline{u^2}$ the increase is quite startling. At first sight it might seem surprising that $\overline{v^2}$ rises across the whole layer right up to reattachment. However, Wood & Bradshaw (1982) have shown that in a plane mixing layer constrained by a solid wall on its *high*-velocity side $\overline{v^2}$ also initially increases across the whole layer. They concluded that the pressure–strain redistribution terms in the transport equations for the normal stresses initially act, under the influence of the wall, to transfer energy *to* the normal component – eventually they must do the opposite because of the impermeability condition at the wall. Most of the rise in $\overline{v^2}$ was found to occur at the low-wavenumber end of the energy spectrum. It is possible that a similar process occurs in the present case but detailed correlation and spectral measurements are required before definite conclusions can be drawn. A significant difference between the two flows is the behaviour of the $\overline{w^2}$ component, which Wood & Bradshaw found to be largely unaffected by the wall – this was one of the facts that led to their conclusion regarding the reason for the surprising rise in $\overline{v^2}$. It may therefore be that, again, the influence of the turbulent fluid returned upstream at reattachment is more dominant in determining the nature of the separated shear layer than any wall effect.

The re-entrainment of returned fluid provides the possibility of 'positive feedback'. If there *is* a tendency for, say, the v-component turbulent energy to be amplified upstream of reattachment, the returned fluid will have a higher energy which, via its entrainment by the upstream flow, will further enhance the energy levels. In the case of the $\overline{v^2}$ component the limit in its continual amplification via this feedback loop

would be provided by the impermeability condition at the wall. There is no similar limit on the transverse energy component which consequently is free to continue rising, relative to $\overline{v^2}$, across the whole layer. Eventually the action of the pressure–strain redistribution terms must prevent it rising too high relative to the other components.

The contrast between the behaviour of $\overline{v^2}$ and $\overline{w^2}$ is further emphasized by their behaviour along the line of maximum $\overline{u^2}$ and along $y/h_f = 0.27$ – quite close to the wall (figure 19*b*). Note that in the latter case the data have *not* been rotated into the β-direction; the streamline plot (figure 9) indicates that the flow is virtually parallel to the wall for $0.2 < x/x_R < 0.8$. Most noticeable is the continuing rise in $\overline{w^2}/\overline{u^2}$ (along $\overline{u^2_{max}}$) practically all the way to the final measuring station, compared with the rapid drop in $\overline{v^2}/\overline{u^2}$ beyond reattachment. Since $\overline{w^2}/\overline{u^2}$ throughout a zero-pressure-gradient boundary layer is less than 0.5, there must clearly be a substantial recovery region, as demonstrated directly by previous workers (e.g. Bradshaw & Wong 1972). The effect of the wall on the $\overline{v^2}$ behaviour beyond reattachment is evidently much more direct than its effect on $\overline{w^2}$.

Along $y/h_f = 0.27$ the 'downstream' flow is in the direction of decreasing x for $x/x_R < 1$; in this sense both $\overline{uv}/\overline{q^2}$ and $\overline{v^2}/\overline{u^2}$ near the wall (figure 19) initially rise with x (between $x/x_R = 1.0$ and 0.7) before falling monotonically towards values that would be typical of those at the same non-dimensional distance from the centreline of a plane mixing layer. These latter values are included in the figures. It is significant that the maximum in $\overline{v^2}/\overline{u^2}$ occurs around $x/x_R = 0.6$ whereas near the centre of the shear layer the peak value does not occur until near reattachment and is noticeably lower than the peak near the wall at $x/x_R = 0.6$. It could be argued that $\overline{v^2}/\overline{u^2}$ simply continues rising along the path taken by the large eddies returned at reattachment (roughly, a mean streamline just inside $\psi = 0$) before the influence of the wall becomes dominant, causing a reduction in $\overline{v^2}$. This ignores the complications caused by axis rotations and relies on the structure of the large eddies remaining, to first order at least, largely unaltered as they undergo reversal of direction near reattachment, which seems at variance with conventional wisdom. Although the mean flow timescale governing this 'eddy reversal' process is significantly smaller than typical turbulence timescales, such arguments cannot therefore be too convincing – rapid changes certainly occur just *downstream* of reattachment. In any case, the behaviour of $\overline{uv}/\overline{q^2}$ seems quite different; the maximum value near the wall is much smaller than the peak in the reattachment region and occurs around $x/x_R = 0.8$, which is where the *minimum* occurs near the shear-layer centreline.

4.2. *Autocorrelations and timescales*

Some typical velocity autocorrelations obtained in the separation region using the pulsed-wire anemometer are shown in figure 20. Note that correlation estimates are not available for the first few lags because of the limitations on the minimum pulsing rate of the probe; this does not in principle prevent the possibility of deducing spectral estimates at higher frequencies (see Castro 1985) but this has not been attempted here. Correlation measurements were obtained at various axial stations and transverse positions within the shear layer and the results used to estimate integral timescales, defining the latter by

$$T_x = \int_0^{\tau'} R(\tau)\,\mathrm{d}\tau, \tag{1}$$

where τ' is the location where $R(\tau)$ first crosses the axis ($\tau' = \infty$ if there is *no* crossing).

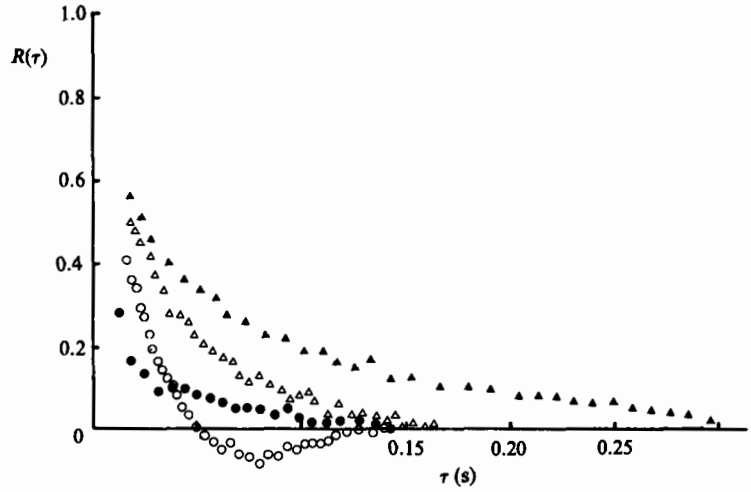

FIGURE 20. Typical velocity autocorrelation functions. ▲, $x/x_R = 0.39$, $y/h_t = 1.6$; △, 0.39, 0.3; ●, 0.51, 2.5; ○, 1.22, 1.6.

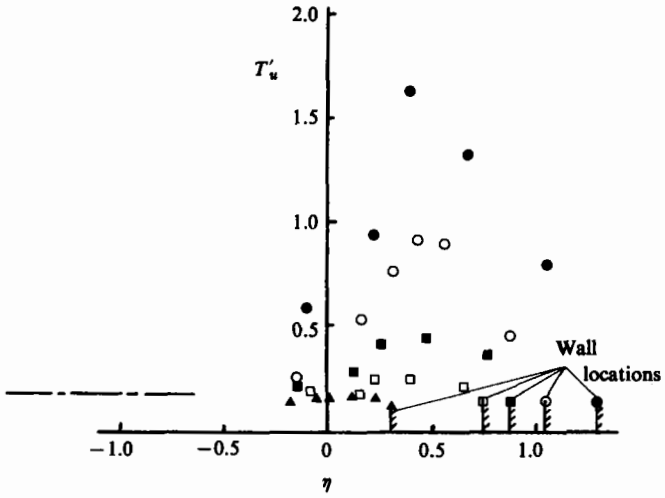

FIGURE 21. Integral timescales, $T'_u = T_x U_r/x$. ●, $x/x_R = 0.41$; ○, 0.52; ■, 0.74, □, 0.96; ▲, 1.24. ——, Kiya & Sasaki (1983) (data at high velocity edge of shear layer).

Figure 21 shows the variation of $T'_u = T_x U_r/x$ at stations between $x/x_R = 0.4$ and 1.24. Kiya & Sasaki (1983) made similar measurements at the outer edge of the shear layer and showed that T_x increased roughly linearly up to reattachment, with $T'_u = 0.18$. This result is included in the figure and the present data extrapolate towards it quite well (correlations were not obtained in the outer part of the flow in the present work). T'_u normally corresponds to the scale of the large vortex structures present in the mixing layer and in the case of the plane-mixing-layer will certainly grow linearly as the flow develops, but its value will depend on the particular definition used for T_x. Some authors choose a timescale based on the time τ' to the crossover point itself (e.g. Wood & Bradshaw 1982) or the time to the first negative peak in $R(\tau)$ (Cherry *et al.* 1984). These will give T'_u values roughly twice and four times the values based on (1), respectively. The latter authors found T'_u values of

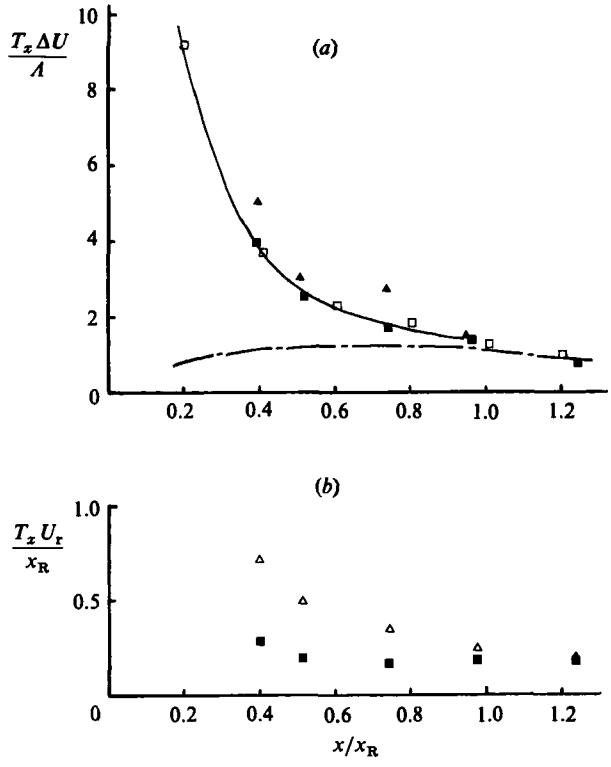

FIGURE 22. Integral timescales. (*a*) ■, $\eta = 0$; ▲, $y/h_t = 0.3$; □, Kiya & Sasaki (1983), $T'_p \Delta U/\Lambda$ (wall pressure); ----, see figure 21. (*b*) △, maximum values; ■, $y/h_t = 0.3$.

around 0.7 from autocorrelations measured at the edge of the flow near reattachment, which is roughly 0.18×4 so is in agreement with the Kiya & Sasaki (1983) result. The present data at $x/x_R = 0.96$ are very similar (figure 21) and indicate a roughly constant value of T'_u across the shear layer.

Further upstream, however, the situation is quite different. Around $\eta = 0$ the timescales are substantially longer than those appropriate to the vortex structures. Figure 22 shows the variation of T_x along $\eta = 0$. Note that on this basis of a normalization using ΔU and Λ the Kiya & Sasaki result for the timescale measured on the edge of the layer is *not* constant, because of the variations of ΔU and Λ with x. Kiya & Sasaki also measured timescales from wall-static-pressure autocorrelations. These are included in figure 22(*a*) and it would seem that at the centre of the shear layer the velocity timescales in the upstream part of the flow are dominated by lower-frequency components as has been previously discussed by Kiya & Sasaki and others (e.g. Cherry *et al.* 1984). This very long timescale component is most noticeable just after separation, where its frequency differs most from that corresponding to the passage (or size) of the vortex structures in the shear layer. Kiya & Sasaki did not present autocorrelations measured near the shear-layer centreline but stated that the v- and w-component timescales were similar and grew roughly like T'_u (at the shear-layer edge) up to reattachment, whereas the longitudinal component was very much larger upstream – agreeing with the present results and the timescales deduced from their wall-pressure measurements.

Typically, previous authors have found the low-frequency component to have a

timescale TU_r/x_R of about 8 near separation, where here T corresponds to the frequency of the peak at the low-frequency end of the velocity (or wall-pressure) spectrum. Since this peak frequency corresponds to the period of the low-frequency oscillations in $R(\tau)$, which is roughly twice the time to the first negative peak on $T(\tau)$ or four times the time to the first crossing, this T corresponds in the present terms to about $8T_x$, so that $T_x U_r/x_R = 1$; this value is consistent with the trend in the data in figure 22(*b*) for decreasing x. Cherry *et al.* (1984) showed that although this time-scale was typical of the overall bubble unsteadiness the spectral peak gradually merges, as the flow develops, with the one corresponding to the large-scale shear-layer structures, so becomes less distinct with increasing x.

The large increases in T'_u across the shear layer (figure 21) are therefore not likely to be a result of drastic changes in large-eddy length-scales, but simply a result of the superposition of the underlying low-frequency component and the more usual mixing-layer eddy structures. The autocorrelation measured at $x/x_R = 0.5$, $y/h_f = 2.5$ provides an example (figure 20). Here the initial decay of $R(\tau)$ would correspond to the usual large-eddy timescales but the measured T'_u is influenced considerably by the delay in the final decay of $R(\tau)$, caused by the presence of the low-frequency component. Note that normalization of T_x by a typical local convection speed, even if the latter could be unambiguously determined, would not be likely to reduce the peaks in figure 21 to levels typical of the usual mixing-layer structures. Although the peaks occur roughly where the local mean velocity is zero, velocity fluctuation levels are of course very high and appropriate convection speeds must also be relatively high. It is, in any case, highly unlikely that the latter would increase by a factor of 1.6 between $x/x_R = 0.41$ and 0.52, which is roughly the ratio of the peak $T_x U_r/x_R$ values at these two stations.

Near the wall the integral timescales are lower than the peak values but still much higher than those appropriate to large-eddy structures in the shear layer. They are also much higher than those typical around reattachment so would again seem to be dominated by the underlying, low-frequency 'flapping' of the shear layer. If this low-frequency motion were not present, one might anticipate timescales similar to those in the fluid returned upstream from the reattachment zone.

It would obviously be very useful to have direct lengthscale information. Such measurements have not as yet been made in separated flows but we are currently developing appropriate pulsed-wire anemometry techniques and hope to obtain useful spatial correlation data shortly.

5. Conclusions

With extensive use of pulsed-wire anemometry we have shown that a separated shear layer bounding a highly turbulent reverse-flow region has many features which are quite different from those of the plane mixing layer between two streams. The shear-layer growth rate is neither closely linear nor equal to that of the plane-mixing-layer, being initially rather higher but reducing gradually as reattachment is approached, by which time it is significantly lower than the plane-mixing-layer value. This is accompanied by a continual rise in turbulence energy all the way to reattachment, followed by a relatively rapid fall thereafter. Although there are significant variations in mean flow direction across the layer, particularly on the low-velocity side where the flow reverses, a distinct shear-layer direction can be identified over a major portion of the flow. Using local coordinate axes aligned with this direction the turbulent shear stress along the flow centreline remains roughly

constant (at a value close to that in the plane mixing layer) up to around $x/x_R = 0.8$, provided it is normalized by the local maximum velocity difference across the layer. It then rises to reach a peak around reattachment before falling again.

The largest changes in the normal and shear stresses occur on the low-velocity side of the layer and the normal stresses around reattachment behave in quite different ways. In particular, the lateral component ($\overline{w^2}$) continues rising all through re-attachment, in contrast to the other components. A major conclusion is that the stabilizing curvature present almost all the way from separation to reattachment does not have a significant influence on the flow. Although the curvature parameter describing the 'strength' of the extra mean strain rate is comparable over much of the flow with the values in the curved mixing layer studied by Castro & Bradshaw (1976), the changes in the turbulence structure are quite different. They would seem to be dominated by the re-entrainment of turbulent fluid returned upstream around reattachment, which provides 'positive feedback' to the separated shear layer. The evidence suggests that one of the reasons for the different behaviour in the normal stresses is that the continual amplification of the vertical component ($\overline{v^2}$), caused by wall influence plus feedback, is limited by the impermeability condition at the wall, whereas no similar restraint occurs for $\overline{w^2}$. The initial rise in $\overline{v^2}$ may be caused by wall influence in a way similar to that described by Wood & Bradshaw (1982).

The longitudinal velocity autocorrelation results imply a behaviour consistent with that described by Castro (1981), Eaton & Johnston (1982), Cherry *et al.* (1984) and Kiya & Sasaki (1983) in four different but related geometries. There is a low-frequency motion of the whole flow on a time-scale much longer than that associated with the usual large-eddy motions in the mixing layer. This is most noticeable near separation where the corresponding spectral peak is well separated from that associated with the shear-layer turbulence. Whilst timescales in the outer flow are similar to those measured in plane mixing layers, near the centre of the shear layer much larger integral timescales are apparent in the first part of the separated region. These are close to those deduced by Kiya & Sasaki and Cherry *et al.* from wall-pressure measurements and fall as reattachment is approached. At $x/x_R = 1.0$ the integral timescale is roughly constant across the whole flow and is associated with the large-eddy motions there, having a value roughly equal to that in the ordinary plane mixing layer. Whilst the autocorrelation measurements are believed to be amongst the first obtained within a reversed-flow region and seem to confirm earlier work, more definite conclusions regarding the role of the large-eddy structures and the causes of the very low-frequency motion must await the availability of detailed spatial correlations, although recent work by Kiya & Sasaki (1985) has been helpful in this respect.

The flow close to the wall within the recirculating region has some features reminiscent of a laminar boundary layer in a favourable pressure gradient. It has been shown that the surface skin friction is Reynolds-number dependent whilst the overall flow is not; a universal collapse of skin-friction data from separated flows of quite different geometry is possible provided appropriate scaling parameters are used. However, whilst the wall layer must be strongly influenced by viscosity, it is difficult to believe that it is 'simply' an unsteady laminar boundary layer. More data of the kind discussed by Adams *et al.* (1984) is required but is difficult to obtain since the scale of the wall region is so small compared with the overall scale of the separated flow.

For the future, we intend to measure some velocity triple products and use more detailed autocorrelation data to deduce spectra. This will allow estimation of most

of the terms in the transport equation for turbulence energy and shed more light on the kinds of turbulence model that might be appropriate for the numerical predictions of such flows. Spatial correlation measurements are also necessary, along with other data to illuminate the unsteady nature of the flow. It may well transpire that the unsteady effects in such separated flows preclude their prediction by *any* model of the time-averaged equations. Hopefully, the present results, in addition to highlighting some of the distinguishing features of a turbulent separated flow, should be useful as test data for current prediction methods.

This work has benefited from helpful discussions with the author's colleagues, principally Dr P. E. Hancock and Dr M. Dianat, which are gratefully acknowledged. The experiments could not have been undertaken without the ongoing support of the technical staff in the Mechanical Engineering Department and the financial support of one of us (A. H.) through a Science and Engineering Research Council Fellowship.

REFERENCES

ADAMS, E. W., JOHNSTON, J. P. & EATON, J. K. 1984 Experiments on the structure of a turbulent reattaching shear layer. *Rep.* MD-43, Thermo-Sciences Div., Dept. Mech. Engng, Stanford University.

ARIE, M. & ROUSE, H. 1956 Experiments on two-dimensional flow over a normal wall. *J. Fluid Mech.* **1**, 129.

BRADBURY, L. J. S. 1976 Measurements with a pulsed wire and hot wire anemometer in the highly turbulent wake of a normal flat plate. *J. Fluid Mech.* **77**, 473.

BRADBURY, L. J. S. & CASTRO, I. P. 1971 A pulsed wire technique for velocity measurements in highly turbulent flows. *J. Fluid Mech.* **49**, 657.

BRADSHAW, P. 1967 The effect of initial conditions on the development of a free shear layer. *J. Fluid Mech.* **26**, 255.

BRADSHAW, P. & WONG, F. Y. F. 1972 Reattachment of a turbulent shear layer. *J. Fluid Mech.* **52**, 113.

BREDERODE, V. A. S. L. DE 1975 Three-dimensional effects in nominally two-dimensional flows. Ph.D. thesis, Imperial College, University of London.

CASTRO, I. P. 1973 A highly distorted turbulent free shear layer. Ph.D. thesis, Imperial College, University of London.

CASTRO, I. P. 1979 Relaxing wakes behind surface-mounted obstacles in rough wall boundary layers. *J. Fluid Mech.* **93**, 631.

CASTRO, I. P. 1981 Measurements in shear layers separating from surface mounted obstacles. *J. Wind. Engng Indust. Aero.* **7**, 253.

CASTRO, I. P. 1985 Time domain measurements in separated flows. *J. Fluid Mech.* **150**, 183.

CASTRO, I. P. 1986 The measurement of Reynolds stresses. In *Encyclopedia of Fluid Mechanics*, p. 1256, Gulf.

CASTRO, I. P. & BRADSHAW, P. 1976 The turbulence structure of a distorted mixing layer. *J. Fluid Mech.* **73**, 265.

CASTRO, I. P. & CHEUN, B. S. 1982 The measurements of Reynolds stresses with a pulsed wire anemometer. *J. Fluid Mech.* **118**, 41.

CASTRO, I. P. & DIANAT, M. 1983 Surface flow patterns on rectangular bodies in thick boundary layers. *J. Wind Engng Indust. Aero.* **11**, 107.

CASTRO, I. P., DIANAT, M. & BRADBURY, L. J. S. 1987 The measurement of fluctuating skin friction with a pulsed wall probe. In *Turbulent Shear Flows* V (ed. F. Durst, B. E. Launder, F. W. Schmidt & J. H. Whitelaw), p. 278. Springer.

CASTRO, I. P. & FACKRELL, J. E. 1978 A note on two-dimensional fence flows with emphasis on wall constraint. *J. Indust. Aero.* **3**, 1.

CHANDRSUDA, C. & BRADSHAW, P. 1981 Turbulent structure of a reattaching layer. *J. Fluid Mech.* **110**, 171.

CHERRY, N. J., HILLIER, R. & LATOUR, M. E. M. P. 1983 The unsteady structure of two-dimensional and reattaching flows. *J. Wind Engng Indust. Aero.* **11**, 95.

CHERRY, N. J., HILLIER, R. & LATOUR, M. E. M. P. 1984 Unsteady measurements in a separated and reattaching flow. *J. Fluid Mech.* **144**, 13.

DEVENPORT, W. J. 1985 Separation bubbles at high Reynolds number: measurement and computation. Ph.D. thesis, University of Cambridge.

DRIVER, D. M. & SEEGMILLER, H. L. 1982 Features of a reattaching turbulent shear layer subject to an adverse pressure gradient. *AIAA* 82-1029.

EATON, J. K. & JOHNSTON, J. P. 1980 Turbulent flow reattachment: an experimental study of the flow and structure behind a backward facing step. *Rep.* MD-39, Thermo-Sciences Div., Dept. Mech. Engng, Stanford University.

EATON, J. K. & JOHNSTON, J. P. 1982 Low frequency unsteadiness of a reattaching turbulent shear layer. In *Turbulent Shear Flows*, vol. III (ed. L. J. S. Bradbury, F. Durst, B. E. Launder, F. W. Schmidt & J. H. Whitelaw), p. 162. Springer.

GOOD, M. C. & JOUBERT, P. N. 1968 Form drag of two-dimensional bluff plates immersed in turbulent boundary layers. *J. Fluid Mech.* **31**, 547.

GREEN, J. E. 1966 Two-dimensional reattachment as a boundary layer problem. *AGARD Conf. Proc.* 4.

JAROCH, M. 1985 Development and testing of pulsed wire probes for measuring fluctuating quantities in highly turbulent flows. *Exp. Fluids* **3**, 315.

KIYA, M. & SASAKI, K. 1983 Structure of a turbulent separation bubble. *J. Fluid Mech.* **137**, 83.

KIYA, M. & SASAKI, K. 1985 Structure of large scale vortices and unsteady reverse flow in the reattachment zone of a turbulent separation bubble. *J. Fluid Mech.* **154**, 463.

KIYA, M., SASAKI, K. & ARIE, M. 1982 Discrete vortex simulation of a turbulent separation bubble. *J. Fluid Mech.* **120**, 209.

KLINE, S. J., CANTWELL, B. J. & LILLEY, G. M. 1982 *The 1980/81 ASOFR–HTTM–Stanford Conference in Complex Turbulent Flows.* Thermo-sciences Div., Dept. Mech. Engng, Stanford University.

MUELLER, T. J. & ROBERTSON, J. M. 1963 In *Modern Developments in Theoretical Applied Mechanics*, vol. 1, p. 326.

PATEL, V. C. 1965 Calibration of the Preston tube and limitations on its use in pressure gradients. *J. Fluid Mech.* **23**, 185.

PLATE, E. 1971 The aerodynamics of shelter belts. *Agri. Met.* **8**, 203.

PRONCHICK, S. W. & KLINE, S. J. 1983 An experimental investigation of the structure of a turbulent reattaching flow behind a backward facing step. *Rep.* MD-42, Thermo-Sciences Div., Dept. Mech. Engng, Stanford University.

RODI, W. 1975 A review of experimental data of uniform density free turbulent boundary layers. In *Studies in Convection*, vol. 1 (ed. B. E. Launder). Academic.

ROSHKO, A. & LAU, J. C. 1965 Some observations on transition and reattachment of a free shear layer in incompressible flow. In *Proc. 1965 Heat Transfer and Fluid Mech. Inst.*

RUDERICH, R. & FERNHOLZ, H. H. 1986 An experimental investigation of a turbulent shear flow with separation, reverse flow and reattachment. *J. Fluid Mech.* **163**, 283

SMITS, A. J. 1982 Scaling parameters for a time-averaged separation bubble. *Trans. ASME* I: *J. Fluids Engng* **104**, 178.

TILLMAN, W. 1945 British Ministry of Aircraft Production, Volkenrode Translation MAP-VG 34-45T

TUTU, N. K. & CHEVRAY, R. 1975 Crossed-wire anemometry in high intensity turbulence. *J. Fluid Mech.* **71**, 785.

WESTPHAL, R. V., EATON, J. K. & JOHNSTON, J. P. 1980 A new prove for measurement of velocity and wall shear stress in unsteady, reversing flow. *Trans. ASME* I: *J. Fluids Engng* **103**, 478.

WESTPHAL, R. V., EATON, J. K. & JOHNSTON, J. P. 1984 Experimental study of flow reattachment in a single sided sudden expansion. *NASA CR*-3765.

WOOD, D. & BRADSHAW, P. 1982 A turbulent mixing layer constrained by a solid surface. Part 1. Measurements before reaching the surface. *J. Fluid Mech.* **182**, 57.